Structural and In-Plane Buckling Analysis of Two-Hinged Ogee Arches

Ghada M. El-Mahdy

Housing and Building National Research Center (HBRC), 87 El-Tahrir St., Dokki, Giza, PC 11511, Egypt
ghadaelmahdy@yahoo.com,

Abstract: The ogee arch consists of a pair of two tangential circular arcs making an arch shape. The geometry of the arch depends on several interrelated variables including the angles subtended by the arcs, the ratio of the radii of the two arcs, and the height of the arch. This paper provides curves for designing the geometry of ogee arches and outlines the structural analysis of two-hinged ogee arches under different cases of loading. A parametric study of the buckling behavior of ogee arches is presented using a finite element eigenvalue buckling analysis for several cases of loading. The results of the buckling analysis are verified through a nonlinear finite element analysis with initial imperfections. It is found that the buckling load is a function of the height-to-base radius of the arch.
[El-Mahdy GM. **Structural and In-Plane Buckling Analysis of Two-Hinged Ogee Arches.** *J Am Sci* 2012;8(9):261-271]. (ISSN: 1545-1003). http://www.jofamericanscience.org. 38

Keywords: Arches; buckling analysis; finite element analysis; geometry; ogee shaped arch

1. Introduction

An arch is a planar structure that spans a space and supports a load. The significance of the arch is that it provides an aesthetically pleasing shape, as well as, theoretically provides a structure which eliminates tensile stresses in spanning a great amount of open space. The forces are mainly resolved into compressive stresses. By using the arch configuration significant spans can be achieved. However, one downside is that an arch pushes outward at the base, and the horizontal reaction force (or *thrust*) needs to be restrained in some way. Arches can be fixed, hinged, or have 3 hinges, as shown in Figure 1. Arches can take several shapes consisting of a combination of lines, arcs of circles, and other curves as shown in Figure 2.

Figure 1. Statical System of Arches.

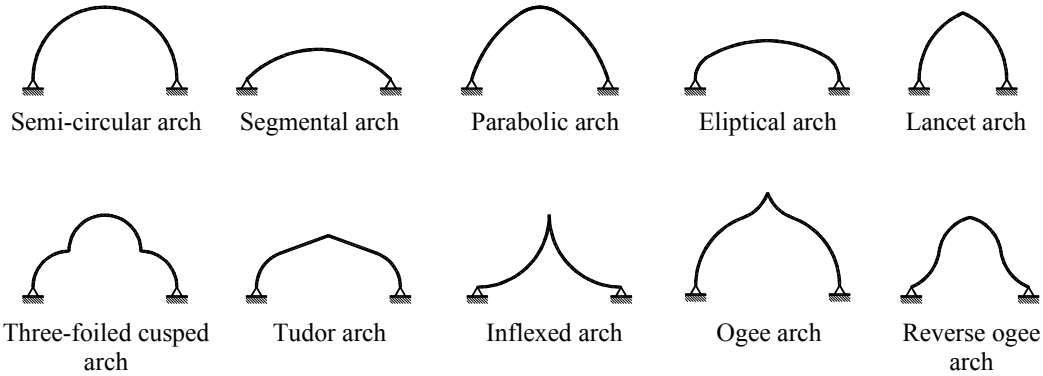

Figure 2. Common Shapes of Arches.

As part of a pilot project on sustainable or green construction at the Housing and Building National Research Center (HBRC) **(El-Mahdy and Zaki, 2010)**, it is proposed to cover the open patio space at the ground floor of HBRC's main building with a self-supporting skin skylight. The HBRC logo consists of an ogee shaped arch with a symbolic sun behind it, hence the new skylight under consideration could take the shape of an ogee arch. The sun symbolizes renewable energy and light, and the arch

itself being symbolic of HBRC's leading role in Egypt in sustainable construction. As there is very little data on ogee arches, the subject of this research is the structural and in-plane buckling analysis of two-hinged ogee shaped arches.

Ogee is a curved shape somewhat like an "S" consisting of two arcs that curve in opposite senses, so that the ends are tangential. In architecture, the term ogee is used for a molding with a profile consisting of a lower concave arc flowing into a convex arc. The ogee arch dates back to ancient Persian and Greek architecture **(Boyd, 1978)** and is also found in Gothic style architecture. Ogee is also a mathematical term meaning "inflection point". In fluid mechanics, the term is used for ogee-shaped aerodynamic profiles, a good example of which is the wing of the Concorde aeroplane. As the upper curves of the ogee arch are reversed, it cannot bear a heavy load. However for the purpose of a self-supporting skin skylight that will only be exposed to its own weight and wind loads, the ogee arch is a suitable solution.

An extensive bibliography on the stability of arches prior to 1970 is given by **DaDeppo and Schmidt (1970)**. The *Handbook of Structural Stability* **(Hayashi, 1971)** gives an overview of results of stability research of arches in which either the equations or graphs of the quoted literature are reproduced. An extensive state-of-the-art report on elastic and inelastic stability of arches is given in **Fukumoto (1996). Singer *et al.* (1998)** provide a chapter on experimental research that has been conducted on arches. **King and Brown (2001)** present a comprehensive study for the practical design of steel curved beams and arches.

Early papers on arch stability devoted to linear stability problems where no bending moments were induced in the arch before buckling were summarized by **Austin (1971), Austin and Ross (1976), and Timoshenko and Gere (1961).** More recent results on the stability of tapered arches are reported by **Wolde-Tinsaie and Foadian (1989).** Nonlinear elastic stability where bending moments are induced in the arch before buckling is handled by **Austin and Ross (1976).** The problem of unsymmetrical loading was studied by **Kuranishi and Lu (1972), Chang (1973), and Harrison (1982).** For the same dead and live load intensities, it was found that unsymmetrically distributed load always governs.

The limit analysis of stocky arches was first presented by **Onat and Prager (1953).** A more recent theoretical method for calculating the plastic collapse load of stocky arches is given by **Spoorenburg *et al.* (2012).** The behaviour of slender arches in pure compression is very much like that of a column and it is common to express the buckling strength of such arches in terms of the axial thrust at the quarter point of the arch using the Euler load **(Ziemian, 2010). Pi and Trahair (1999) and Pi and Bradford (2004)** studied the in-plane inelastic stability of hinged and fixed circular arches with I-shape cross sections with different load cases and subtended angles. Other nonlinear buckling studies on arches were made by **Pi and Trahair (1998), Pi *et al.* (2007), and Yau and Yang (2008).**

International building standards are compared with each other in *Stability of Metal Structures, a World View* **(Beedle, 1991). The Eurocode 3, Part 2 (2006)** provides charts with effective length factors for the elastic in-plane buckling of circular, parabolic, and catenary arches with unmovable supports and several articulations. For tied arches with vertical hangers, effective lengths are also given, as is a criterion which indicates if the arch is prone to snap-through buckling. **AASHTO (2004)** provides effective-length factors for fixed, two-hinged and three-hinged arches with rise-to-span ratios of 0.1 to 0.4.

2. Geometry of Ogee Arch

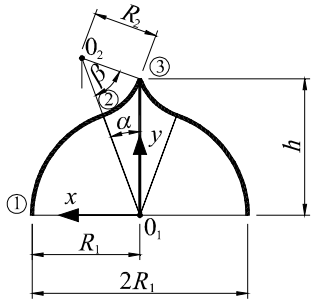

Figure 3. Geometry of Ogee Arch.

The ogee arch is composed of a pair of two discrete circular arcs with independent radii. Hence, there are many geometrical variables to be determined namely, the radius of the lower arc which is half the span of the arch, R_1, the radius of the upper arc, R_2, the angle subtended by the lower arc, 90-α, the angle subtended by the upper arc, β, as well as the overall height of the arch, h. These variables are shown in Figure 3. From the geometry of the arch the coordinates of the peak of the arch, point 3, can be expressed as

$$x_3 = (R_1 + R_2)\sin\alpha - R_2\sin(\alpha+\beta) = 0 \qquad (1)$$

$$y_3 = (R_1 + R_2)\cos\alpha - R_2\cos(\alpha+\beta) = h \qquad (2)$$

Eliminating R_1 from these two simultaneous equations and simplifying gives the expression for R_2/h as

$$\frac{R_2}{h} = \frac{\sin\alpha}{\sin\beta} \qquad (3)$$

Substituting Equation (3) into Equation (1) and simplifying gives the expression for R_1/h as

$$\frac{R_1}{h} = \frac{\sin(\alpha+\beta)-\sin\alpha}{\sin\beta} \quad (4)$$

The radius of the upper curve R_2 can be expressed in terms of R_1, α, and β as

$$\frac{R_2}{R_1} = \frac{\sin\alpha}{\sin(\alpha+\beta)-\sin\alpha} \quad (5)$$

Equations (3) – (5) must be solved iteratively to determine all the geometric variables of an ogee arch, so to simplify the process of design the graphs in Figures 4 and 5 have been developed to determine the geometric variables for a specific height-to-half span ratio, h/R_1. Figure 4 plots the relationship between the ratio h/R_1 for different values of angle α such that angle β can be determined from these independent variables. Figure 5 plots the relationship between the ratio h/R_1 for different values of angle α such that the ratio R_2/R_1 can be determined. It is to be noted that Eqs. (3) – (5) are only valid for practical values of h/R_1 as for higher ratios the left and right curves of the arch overlap each other suggesting that there are two solutions to the problem a practical one and an imaginary one.

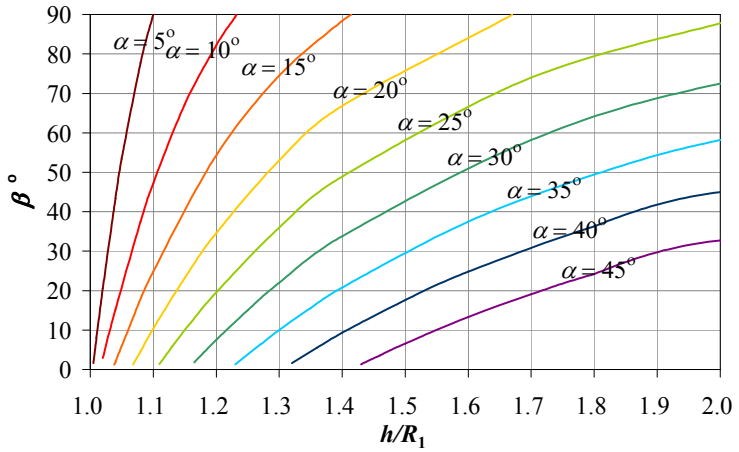

Figure 4. Relationship of h/R_1 Versus Angle β.

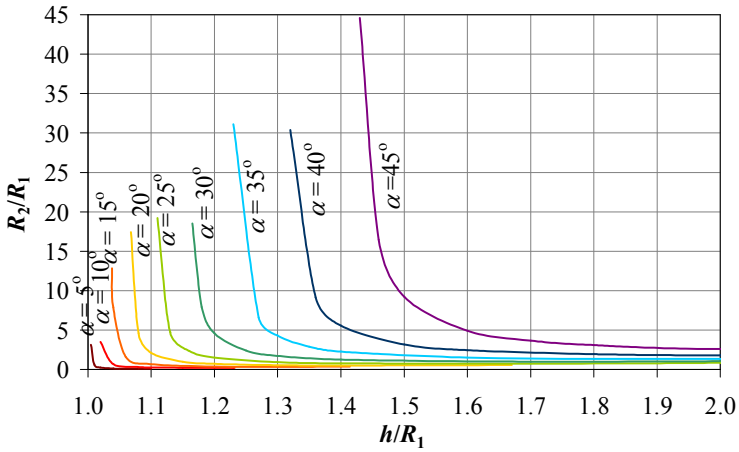

Figure 5. Relationship of h/R_1 Versus R_2/R_1.

3. Structural Analysis of Ogee Arch

Arches behave like two-dimensional beams spanning an open space, but unlike simple beams arches have a horizontal thrust resisting the tendency of the arch to open out. The common statical systems of an arch can be either a three-hinged arch, a two-hinged arch, or a fixed-fixed arch as shown in Figure 1. For most common arch applications the two-hinged arch is the most practical and is the statical system used in this research.

3.1 Horizontal Thrust

The arch is assumed to be a two hinged arch with horizontal base reactions H, as shown in Figure

6. To analyze this arch the principal of virtual work **(Williams, 2009)** or minimum strain energy (**Timoshenko, 1930**) is used giving the horizontal support reaction as

$$H = \frac{\int Myds / EI}{\int y^2 ds / EI} \qquad (6)$$

where M is the bending moment of the applied load case for a statically determinate simply supported arch, y is the distance from the base of the arch and represents the bending moment due to a unit horizontal load applied at the released support of the statically determinate simply supported arch, ds is the infinitesimal distance along the length of the arch, and EI is the bending rigidity of the arch (E being the modulus of elasticity and I the moment of inertia of the cross-section about the axis of bending). For the ogee arch, two circular coordinate systems are required as shown in Figure 6; the first for the lower part of the arch using θ as the variable and integrating the moments from $\theta = \alpha$ to $\theta = \pi/2$, and the second for the upper part of the arch using ϕ as the variable and integrating the moments from $\phi = \alpha$ to $\phi = (\alpha + \beta)$. The horizontal reaction that prevents the spread of the arch depends on the type of loading applied to the arch. Three cases of loading are analysed namely a concentrated load P at the peak of the arch (midspan), a uniformly distributed vertical load acting along the horizontal projection w, and a uniformly distributed horizontal load acting along the vertical projection w_h, which are shown in Figure 7.

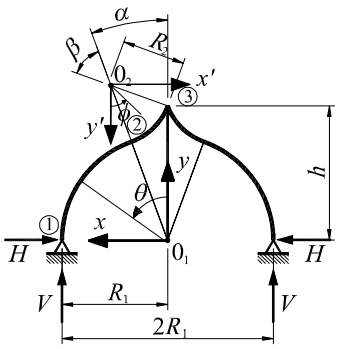

Figure 6. Statical System of Two-Hinged Ogee Arch.

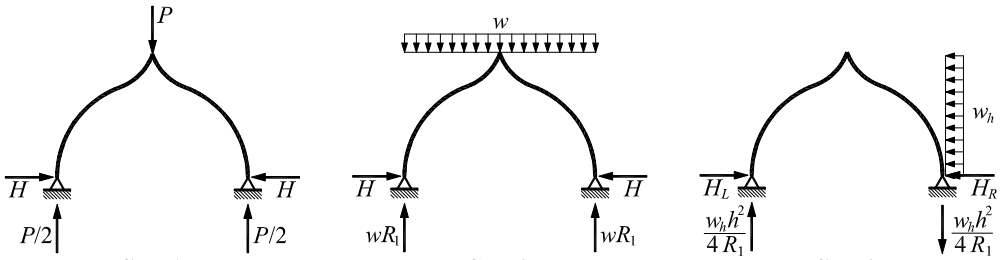

Figure 7. Load Cases Considered in Structural Analysis for Horizontal Thrust Reaction.

3.1.1. Case (1): Concentrated Load at Midspan

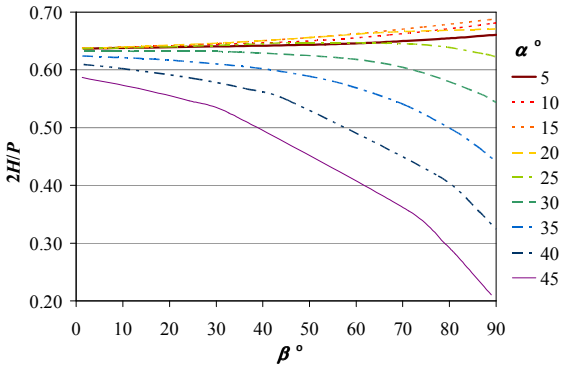

Figure 8. Horizontal Thrust for Case 1 Loading, Concentrated Load P at Midspan.

Due to the complexity of the expression derived for the horizontal thrust it is not stated here but is given in the appendix. The value of the horizontal reaction for a concentrated load P at midspan is plotted in Figure 8 in the nondimensional form of $2H/P$ for different values of angles α and β. It can be seen that for the arches with angles of α between 5° and 20°, the horizontal thrust increases slightly with the increase in the height-to-span ratio (*i.e.*, increase of β), whereas for values of α between 25° and 45°, the horizontal thrust decreases with the increase of this ratio.

3.1.2. Case (2): Uniformly Distributed Vertical load Acting Along Horizontal Projection

For a uniformly distributed vertical load of w acting along the horizontal projection the horizontal reaction, the expression for which is given in the appendix, is plotted in Figure 9 in the nondimensional form of $3H/2wR_1$ for different values of angles α and β. It can be seen that for all values of α, the horizontal thrust decreases with the increase in the height-to-span ratio, however, this decrease becomes significantly greater as α increases.

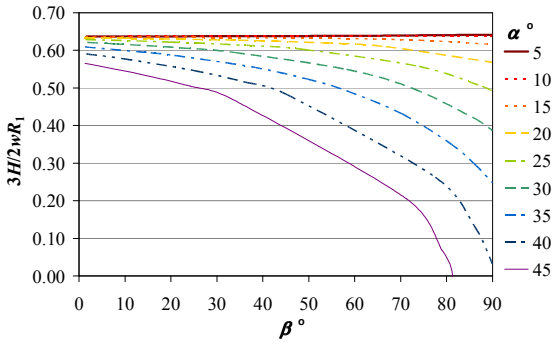

Figure 9. Horizontal Thrust for Case 2 Loading, Uniformly Distributed Vertical Load w.

3.1.3. Case (3): Uniformly Distributed Horizontal Load Acting Along Vertical Projection

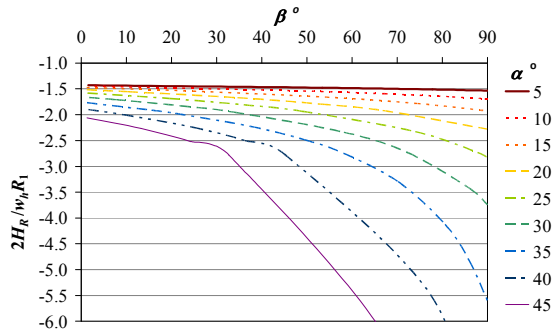

Figure 10. Horizontal Thrust for Case 3 Loading, Uniformly Distributed Horizontal Load w_h.

For a uniformly distributed horizontal load of w_h acting along the vertical projection the horizontal reaction on the side of the horizontal loading (*i.e.*, the right side), the expression for which is given in the appendix, is plotted in Figure 10 in the nondimensional form of $2H_R/w_hR_1$ for different values of angles α and β. Again, it can be seen that for all values of α, the horizontal thrust decreases with the increase in the height-to-span ratio, however, this decrease becomes significantly greater as α increases.

3.2 Bending Moment

Arch-type structures are most efficient if they carry their load in such a way that the funicular curve coincides with the centroidal axis, which results in axial compression and no bending of the arch axis **(Ziemian, 2010).** Examples of arches under pure axial compression include circular arches subjected to uniform normal pressure, commonly called hydrostatic loading, parabolic arches subjected to uniform load on a horizontal projection, and catenary arches with load uniformly distributed along the arch axis. However, for other shapes of arches and other types of loading, a small amount of bending moment will occur along the axis of the arch. Hence, arches are generally designed to resist axial compression forces and small amounts of moments.

4. In-Plane Buckling of Arches

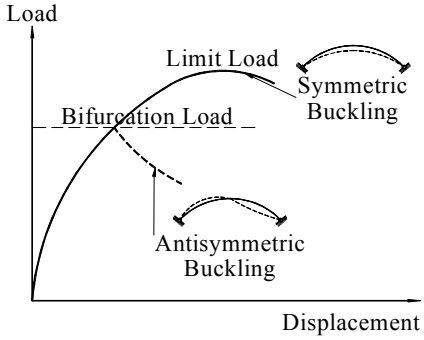

Figure 11. Modes of In-Plane Buckling of Arches.

The stability of an arch can be characterized by buckling in or out of the plane of the arch. In-plane buckling occurs when the arch is substantially braced against out-of-plane deformations, while out-of-plane buckling occurs for arches with significant free-standing portions. In-plane buckling is associated with combined compression and bending while out-of-plane buckling is associated with combined compression, biaxial bending, and torsion. This paper deals with in-plane buckling. Arches can buckle in-plane in a symmetrical buckling mode or an antisymmetrical buckling mode, as shown in Figure 11 **(Ziemian, 2010).** Generally, the symmetrical buckling load is greater than the antisymmetrical buckling load. If an antisymmetric mode does not become dominant, the arch eventually becomes unstable in a symmetrical mode with the load-deflection curve gradually reaching a limit point. On the other hand, the limit load may be significantly reduced if an antisymmetrical buckling mode dominates. This antisymmetric bifurcation load is the subject of discussion in this paper.

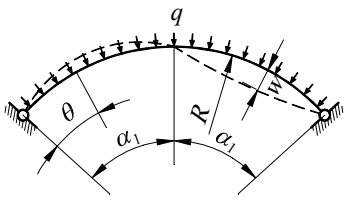

Figure 12. Buckling of an Arch.

The buckling of arches is well presented by **Timoshenko and Gere (1961)**. The radial deflection of a circular arch of radius R and subjected to a uniform pressure is taken as w, as shown in Figure

12. The moment in the arch is assumed to be equal to the secondary moment due to the internal compressive force, S, multiplied by the deflection w (*i.e.*, $M = Sw$). Hence, the differential equation for the buckling of the arch is

$$\frac{d^2w}{d\theta^2} + w = -\frac{R^2Sw}{EI} \qquad (7)$$

where $S = qR$, q being the uniform pressure acting on the arch, and EI is the bending rigidity of the arch. In this equation the variation of the compressive force S along the length of the arch is neglected. Taking $k^2 = 1 + qR^3/EI$ the differential equation for the buckling of the circular arch becomes

$$\frac{d^2w}{d\theta^2} + k^2w = 0 \qquad (8)$$

The general solution of this equation is $w = A \sin k\theta + B \cos k\theta$. Satisfying the condition at the left end ($\theta = 0$) gives $B = 0$, and the condition at the right end ($\theta = 2\alpha_1$) gives $\sin 2\alpha_1 k = 0$. The smallest root for this that satisfies the condition of inextensibility of the center line of the arch is $k = \pi/\alpha_1$ giving

$$q_{cr} = \frac{EI}{R^3}\left(\frac{\pi^2}{\alpha_1^2} - 1\right) \qquad (9)$$

Equation (9) is also a good approximation for the case of a uniformly distributed vertical load. **Austin (1971)** noted that the critical thrust for the case of a two-hinged circular arch with midspan concentrated load in which large bending moment and displacements exist prior to buckling is nearly the same as the critical thrust for the uniform pressure loading which causes only compression in the arch. So, it can be assumed that the buckling data for arches subjected to loadings which cause pure compression can be used to estimate the critical loading values for other symmetrical loadings.

5. Finite Element Analysis

COSMOS/M 2.6, a finite element program, was used to model the ogee arches. The finite element model consisted of 2D elastic straight beam elements along the axis of the arch. The beam elements were modeled using the properties of steel giving the material model a modulus of elasticity of 210 GPa and a yield stress of 350 MPa. The model was given a cross-sectional area of 8450 mm^2 and a moment of inertia of 0.231 x 10^9 mm^4. The model was constrained at the base of the arch in both planar directions to achieve the pinned-end conditions. Initially, a linear analysis was conducted to verify the horizontal reactions derived previously and to obtain the bending moment diagram. Then an eigenvalue buckling analysis was conducted to find the trend in elastic buckling for each case of loading. A nonlinear analysis was conducted to verify these elastic buckling loads.

Table 1. Specimens Used in Parametric Study.

Specimen	Angle α^o	h/R_1	Angle β^o	R_2/R_1	Specimen	Angle α^o	h/R_1	Angle β^o	R_2/R_1
S1	0	1.000	0.0	0.000	S22	25	1.400	48.9	0.785
S2	5	1.005	1.6	3.137	S23	30	1.165	1.8	18.545
S3	5	1.050	53.4	0.114	S24	30	1.200	7.5	4.597
S4	5	1.080	77.8	0.096	S25	30	1.300	22.0	1.735
S5	5	1.100	90.0	0.096	S26	30	1.400	33.8	1.258
S6	10	1.020	2.9	3.501	S27	30	1.700	58.2	1.000
S7	10	1.100	47.2	0.260	S28	35	1.230	1.3	31.097
S8	10	1.150	67.2	0.217	S29	35	1.350	15.6	2.879
S9	10	1.200	82.2	0.210	S30	35	1.400	20.8	2.261
S10	15	1.038	1.2	12.828	S31	35	1.600	37.5	1.508
S11	15	1.100	24.8	0.679	S32	35	1.800	49.4	1.360
S12	15	1.200	54.3	0.383	S33	35	2.000	58.2	1.350
S13	15	1.300	74.5	0.349	S34	40	1.320	1.6	30.388
S14	20	1.068	1.2	17.442	S35	40	1.400	9.3	5.569
S15	20	1.100	10.3	2.104	S36	40	1.600	24.8	2.452
S16	20	1.200	34.6	0.723	S37	40	1.800	36.3	1.954
S17	20	1.300	53.0	0.557	S38	40	2.000	45.0	1.818
S18	20	1.400	66.8	0.521	S39	45	1.430	1.3	44.570
S19	25	1.110	1.4	19.200	S40	45	1.600	13.3	4.918
S20	25	1.200	19.6	1.512	S41	45	1.800	24.2	3.105
S21	25	1.300	36.0	0.935	S42	45	2.000	32.7	2.618

The parametric study consisted of 42 specimens with angles α ranging from 0^o to 45^o and h/R_1 ratios ranging from 1 to 2. The corresponding values of angle β and ratio R_2/R_1 were determined from Equations (3) – (5). These specimens represent ogee arches of practical proportions with various height and curvature. The lower bound of these specimens, S1, was a semi-circular arch with $\alpha = 0^o$ and h/R_1 equal to 1. This specimen was used to compare the finite element results with the theoretical buckling results and also represented the upper limit for the bifurcation buckling loads of the ogee arches. Table 1 lists the specimens used in the parametric study.

6. Results and Discussion

6.1. Linear Analysis

The linear analysis was used to verify the horizontal thrust reactions shown in Figures 8 – 10 and analytically stated in the appendix, and to obtain the bending moment diagrams. The finite element horizontal thrust compared accurately with the analytical values derived with a deviation of less than 0.5% for Case 1 loading, less than 0.3% for Case 2 loading, and less than 5% for Case 3 loading. The deformed shape and bending moments for the three cases of loading are shown in Figure 13 (a) – (c). As the ogee curve is not the funicular curve for any of these cases of loading, there is a fair amount of bending moment produced, which must be taken into consideration in the design of such arches.

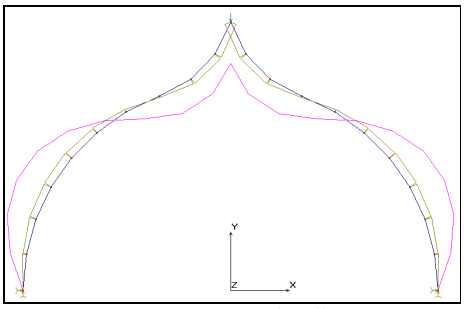

(a) Case 1 loading.

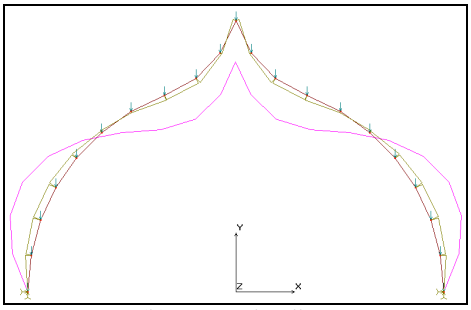

(b) Case 2 loading.

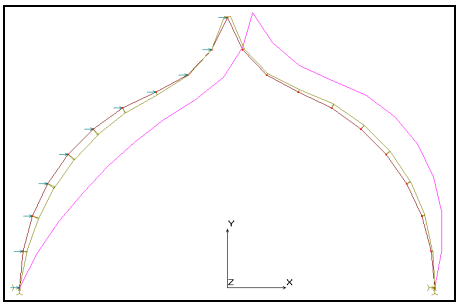

(c) Case 3 loading.

Figure 13. Deflected Shape and Bending Moment Diagram for the Three Cases of Loading.

6.2. Eigenvalue Buckling Analysis

The critical value of the uniform pressure, q_{cr}, is $3EI/R^3$ in accordance with the theoretical results for a two-hinged semicircular arch ($\alpha_1 = \pi/2$) subjected to uniform pressure as given in Equation (9). Using the finite element method to perform an eigenvalue buckling analysis the bifurcation uniform pressure was found to equal $3.27EI/R^3$ for a two-hinged uniformly compressed semicircular arch with constant cross section. Furthermore, the bifurcation load was found to equal $3.50EI/R^3$ for a two-hinged semicircular arch with constant cross section and loaded by a uniformly distributed vertical load acting along the horizontal projection (*i.e.*, live load), and $2.62EI/R^3$ for a two-hinged semicircular arch with constant cross section and loaded by a uniform vertical pressure acting along the axis of the arch (*i.e.*, dead load). Hence, the finite element buckling analysis compares relatively well with the theoretical values. The bifurcation buckling mode is antisymmetrical as shown in Figure 14.

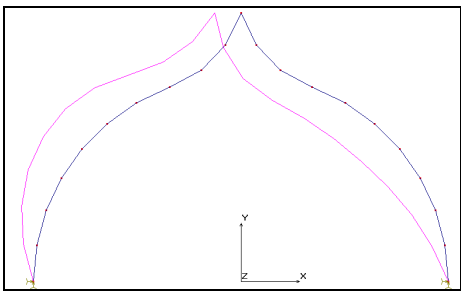

Figure 14. Antisymmetrical Buckling Mode of Arch.

6.3. Nonlinear Analysis

To verify the bifurcation loads obtained from the buckling analysis, a nonlinear analysis was conducted with an initial geometric imperfection. The arch was modeled with an initial horizontal imperfection at the peak of the arch and the load was

applied incrementally using elastic material properties and large deformation. The load converged with the bifurcation load in an antisymmetrical deformation mode which tended to push the arch in the opposite direction to the initial imperfection. Figure 15 shows a typical nonlinear load – horizontal displacement curve for specimen S17 with uniform vertical loading acting along the horizontal projection. The nonlinear analysis indicates a little imperfection sensitivity by showing a slight decrease in the convergence load from the bifurcation buckling load.

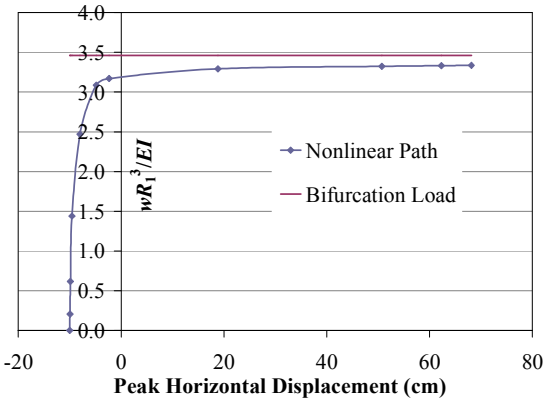

Figure 15. Nonlinear Load – Horizontal Displacement Curve.

6.4. Effect of Height-to-Base Radius Ratio

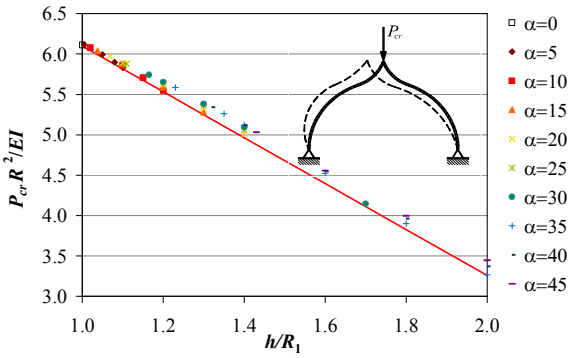

Figure 16. Buckling Load for Concentrated Load at Midspan.

The parametric ogee arch analysis shows that the bifurcation buckling load for the case of a concentrated load at midspan depends only on the ratio of the height of the arch to the radius of the base of the arch (h/R_1). This value can be expressed in a nondimensional form using $P_{cr}R_1^2/EI$ such that the expression

$$\frac{P_{cr}R_1^2}{EI} = -2.84\frac{h}{R_1} + 8.94 \qquad (10)$$

gives a good lower bound solution for this case as shown in Figure 16. The objective of using a nondimensional form is to eliminate the size of the arch, the material properties, and the cross-sectional inertia from the results. In this way the buckling values or Equation (10) can be used to find the buckling load of any size arch with any cross section or material properties.

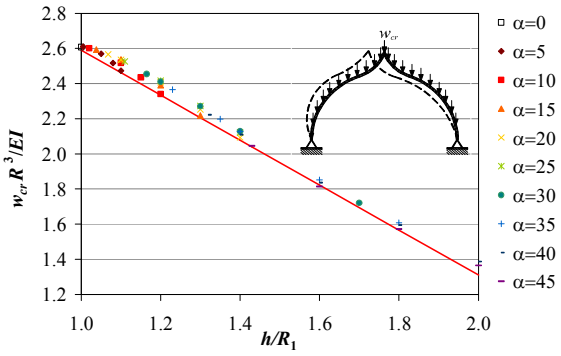

Figure 17. Buckling Load for Uniformly Distributed Vertical Load Acting Along the Axis of the Arch.

For the case of uniformly distributed vertical loading acting along the axis of the arch, representing the dead load, the parametric ogee arch analysis shows that the buckling load again depends only on the ratio of the height of the arch to the radius of the base of the arch (h/R_1). This value can be expressed in a nondimensional form using $w_{cr}R_1^3/EI$ such that the expression

$$\frac{w_{cr}R_1^3}{EI} = -1.28\frac{h}{R_1} + 3.87 \qquad (11)$$

gives a good lower bound solution for this case as shown in Figure 17.

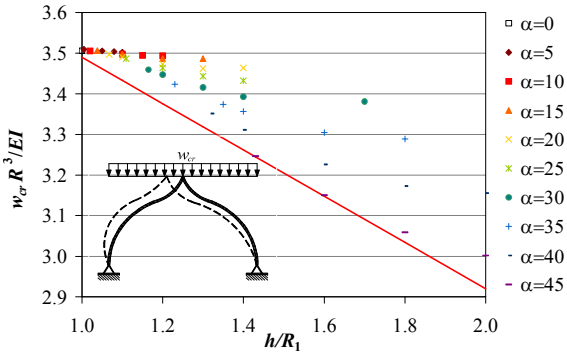

Figure 18. Buckling Load for Uniformly Distributed Vertical Load Acting Along the Horzl. Projection.

The live load distribution is best represented by uniformly distributed vertical loading acting along

the horizontal projection. In this case the parametric ogee arch analysis shows that the buckling load again depends on the ratio of the height of the arch to the radius of the base of the arch (h/R_1) but the relationship is not quite linear and the results show a fair amount of scatter. Figure 18 shows that the lower bound solution for the critical load for this case can be expressed as

$$\frac{w_{cr}R_1^3}{EI} = -0.57\frac{h}{R_1} + 4.06 \qquad (12)$$

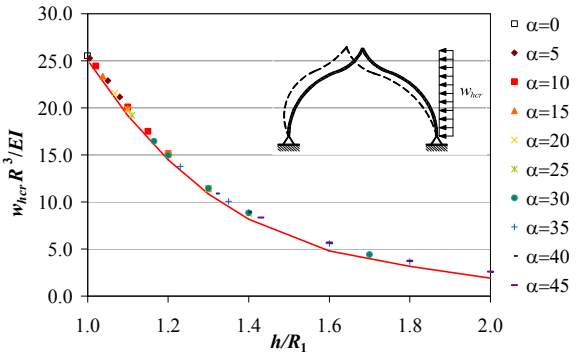

Figure 19. Buckling Load for Uniformly Distributed Horizontal Load Acting Along the Vert. Projection.

Finally, for the horizontal distributed load acting along the vertical projection which represents wind load, the parametric ogee arch analysis shows that the buckling load again depends only on the ratio of the height of the arch to the radius of the base of the arch (h/R_1), but for this case of loading the relationship is nonlinear. The value of the bifurcation buckling load can be expressed in a nondimensional form using $w_{hcr}R_1^3/EI$ such that the expression

$$\frac{w_{hcr}R_1^3}{EI} = -26.9\left(\frac{h}{R_1}\right)^3 + 150.3\left(\frac{h}{R_1}\right)^2 - 285.8\frac{h}{R_1} + 187.5 \qquad (13)$$

gives a good lower bound solution for the critical load for this case as shown in Figure 19.

7. Conclusion

The paper presents the structural and in-plane buckling analysis of two-hinged ogee arches. The geometry of ogee arches are composed of a number of interrelated variables that can be determined from the design curves presented before the analysis can be conducted. The horizontal thrust reaction of two-hinged ogee arches depends on the geometry of the arch and type of loading and, in general, decreases with the increase in height-to-span ratio. The eigenvalue buckling analysis predicted an antisymmetric mode of buckling, which was verified by the nonlinear analysis of the arch with initial geometric imperfections. The bifurcation load of ogee arches depends only on the height-to-base radius ratio, decreasing with the increase in the height-to-base radius ratio. The relationship between the bifurcation load and the height-to-base radius ratio is linear for concentrated midspan loads and uniform vertical loading acting along the axis of the arch. There is a fair amount of scatter in this relationship for uniform vertical loading acting along the horizontal projection, and this relationship is nonlinear for uniform horizontal loading acting along the vertical projection.

8. Appendix

The analytical results for the horizontal thrust for the three cases of loading described in Section 3.1 are as follows:

Case (1): Concentrated Load at Midspan

$$H = \frac{\frac{1}{2}P(A_1 + 4B_1)}{C_1 + 4D_1} \qquad (14)$$

where

$$A_1 = 3 - 4\sin\alpha - \cos 2\alpha$$

$$B_1 = \frac{\frac{1}{2}\beta(1-\sin\alpha)\sin 2\alpha}{\sin(\alpha+\beta)-\sin\alpha} + \left(\frac{\sin\alpha}{\sin(\alpha+\beta)-\sin\alpha}\right)^2\left[\begin{array}{l}\beta(\cos\alpha-\sin 2\alpha)+\sin\alpha+\cos 2\alpha \\ -\sin(\alpha+\beta)-\cos(2\alpha+\beta)\end{array}\right]$$

$$+\left(\frac{\sin\alpha}{\sin(\alpha+\beta)-\sin\alpha}\right)^3\left[\frac{3}{4}\cos 2\alpha - \frac{1}{2}\beta\sin 2\alpha - \cos(2\alpha+\beta) + \frac{1}{4}\cos 2(\alpha+\beta)\right]$$

$$C_1 = \pi - 2\alpha - \sin 2\alpha$$

$$D_1 = \frac{\beta\cos^2\alpha\sin\alpha}{\sin(\alpha+\beta)-\sin\alpha} + 2\cos\alpha\left(\frac{\sin\alpha}{\sin(\alpha+\beta)-\sin\alpha}\right)^2\left[\beta\cos\alpha+\sin\alpha-\sin(\alpha+\beta)\right]$$
$$+\left(\frac{\sin\alpha}{\sin(\alpha+\beta)-\sin\alpha}\right)^3\left[\tfrac{1}{2}\beta(1+2\cos^2\alpha)+\tfrac{3}{4}\sin 2\alpha-2\cos\alpha\sin(\alpha+\beta)+\tfrac{1}{4}\sin 2(\alpha+\beta)\right]$$

Case (2): Uniformly Distributed Vertical load Acting Along Horizontal Projection

$$H = \frac{2wR_1(E_1+3F_1)}{3(C_1+4D_1)} \tag{15}$$

where

$$E_1 = 2-3\sin\alpha+\sin^3\alpha$$

$$F_1 = \frac{\beta\cos^3\alpha\sin\alpha}{\sin(\alpha+\beta)-\sin\alpha} + \left(\frac{\sin\alpha}{\sin(\alpha+\beta)-\sin\alpha}\right)^2\begin{bmatrix}\beta(\cos\alpha-\tfrac{3}{2}\sin\alpha\sin 2\alpha)-\sin 2\alpha\cos(\alpha+\beta)\\+\sin 2\alpha\cos\alpha+\sin^2\alpha\sin(\alpha+\beta)-\sin^3\alpha\\-\sin(\alpha+\beta)+\sin\alpha\end{bmatrix}$$
$$+\left(\frac{\sin\alpha}{\sin(\alpha+\beta)-\sin\alpha}\right)^3\begin{bmatrix}\tfrac{1}{2}\beta(-\cos\alpha-3\sin 2\alpha\sin\alpha)+\tfrac{1}{4}\sin 2(\alpha+\beta)\cos\alpha+\tfrac{7}{4}\sin 2\alpha\cos\alpha\\-2\sin 2\alpha\cos(\alpha+\beta)+\tfrac{1}{2}\sin\alpha\cos 2(\alpha+\beta)-\tfrac{1}{2}\sin\alpha\cos 2\alpha\\+2\sin^2\alpha\sin(\alpha+\beta)-2\sin^3\alpha\end{bmatrix}$$
$$-\left(\frac{\sin\alpha}{\sin(\alpha+\beta)-\sin\alpha}\right)^4\begin{bmatrix}\tfrac{1}{2}\beta\cos\alpha(1+2\sin^2\alpha)-\tfrac{1}{4}\sin 2(\alpha+\beta)\cos\alpha-\tfrac{3}{4}\sin 2\alpha\cos\alpha\\+\sin 2\alpha\cos(\alpha+\beta)-\tfrac{1}{3}\sin^3(\alpha+\beta)+\tfrac{4}{3}\sin^3\alpha-\tfrac{1}{2}\sin\alpha\cos 2(\alpha+\beta)\\+\tfrac{1}{2}\sin\alpha\cos 2\alpha-\sin^2\alpha\sin(\alpha+\beta)\end{bmatrix}$$

Case (3): Uniformly Distributed Horizontal Load Acting Along Vertical Projection

$$H_R = \frac{w_h R_1(G_1+2H_1)}{2(C_1+4D_1)} \tag{16}$$

where

$$G_1 = \chi(2\alpha-\pi+\sin 2\alpha)-4/3+2\sin\alpha-2\sin^3\alpha$$

$$H_1 = \frac{\beta\cos^2\alpha\sin\alpha\left[-2\chi-\cos\alpha\right]}{\sin(\alpha+\beta)-\sin\alpha} + \left(\frac{\sin\alpha}{\sin(\alpha+\beta)-\sin\alpha}\right)^2\cos\alpha\begin{bmatrix}\beta\cos\alpha(-4\chi-3\cos\alpha)\\+4\chi\sin(\alpha+\beta)-4\chi\sin\alpha\\+3\cos\alpha\sin(\alpha+\beta)-\tfrac{3}{2}\sin 2\alpha\end{bmatrix}$$
$$+\left(\frac{\sin\alpha}{\sin(\alpha+\beta)-\sin\alpha}\right)^3\begin{bmatrix}\beta(-2\chi\cos^2\alpha-\chi-3\cos^3\alpha-\tfrac{3}{2}\cos\alpha)+4\chi\cos\alpha\sin(\alpha+\beta)\\-2\chi\sin 2\alpha-\tfrac{1}{2}\chi\sin 2(\alpha+\beta)+\tfrac{1}{2}\chi\sin 2\alpha+6\cos^2\alpha\sin(\alpha+\beta)\\-6\cos^2\alpha\sin\alpha-\tfrac{3}{4}\cos\alpha\sin 2(\alpha+\beta)+\tfrac{3}{4}\cos\alpha\sin 2\alpha\end{bmatrix}$$
$$-\left(\frac{\sin\alpha}{\sin(\alpha+\beta)-\sin\alpha}\right)^4\begin{bmatrix}\beta\cos\alpha(\cos^2\alpha+\tfrac{3}{2})-3\cos^2\alpha\sin(\alpha+\beta)+\tfrac{3}{4}\cos\alpha\sin 2(\alpha+\beta)\\+\tfrac{3}{4}\cos\alpha\sin 2\alpha-\sin(\alpha+\beta)+\sin\alpha+\tfrac{1}{3}\sin^3(\alpha+\beta)-\tfrac{1}{3}\sin^3\alpha\end{bmatrix}$$

$$\chi = \frac{\sin\beta}{\sin(\alpha+\beta)-\sin\alpha}$$

Corresponding Author:
Dr. Ghada M. El-Mahdy
Structures and Metallic Construction Research Institute,
Housing and Building National Research Center (HBRC)
87 El-Tahrir St., Dokki, Giza, PC 11511, PO Box 1770, Cairo, Egypt,
Email:ghadaelmahdy@yahoo.com

References

[1] AASHTO. LRFD Bridge Design Specifications. American Association of State Highway and

Transportation Officials. Washington DC, USA. 2004.
[2] Austin WJ. In-plane bending and buckling of arches. ASCE J Struct Div 1971; 97(5):1575-92.
[3] Austin WJ, Ross TJ. Elastic buckling of arches under symmetrical loading. ASCE J Struct Div 1976; 102(5):1085-95.
[4] Beedle LS (Ed.). Stability of metal structures, a world view. 2nd Ed. Structural Stability Research Council. Bethlehem, PA, USA. 1991.
[5] Boyd TD. The arch and the vault in Greek architecture. Amer J of Archaeology 1978; 82(1):83-100.
[6] Chang CK. Effect of loaded length on the buckling strength of slender arches. Thesis Rice University. Houston, TX, USA.1973.
[7] DaDeppo DA, Schmidt R. Stability of an arch under combined loads, bibliography on stability of arches. Ind Math 1970; 20(2):71-89.
[8] El-Mahdy GM, Zaki MA. How steel can contribute to green building design and maintenance. Proc ASCE 6th Int Engng and Const Conf (IECC'6). Cairo, Egypt; June 28-30 2010.
[9] Eurocode 3. EN 1993-2. Design of steel structures, part 2: steel bridges. European Committee for Standardization (CEN). Brussels, Belgium. 2006.
[10] Fukumoto Y. Structural stability design, steel and composite structures. Pergamon. Amsterdam, Netherlands.1996.
[11] Harrison HB. In-plane stability of parabolic arches. ASCE J Struct Div 1982; 108(ST1):195-205.
[12] Hayashi T. (Ed.). Handbook of structural stability. Corona Publishing. Tokyo, Japan. 1971.
[13] King C, Brown D. Design of curved steel. Steel Construction Institute. Ascot Berks, UK. 2001.
[14] Kuranishi S, Lu LW, Load carrying capacity of two-hinged steel arches. Proc Jpn Soc Civ Eng 1972; (204):129-40.
[15] Onat ET, Prager W. Limit analysis of arches. J Mech Phys Solids 1953; 1:71-89.
[16] Pi YL, Bradford MA. In-plane strength and design of fixed steel I-section arches. Eng Struct 2004; 26(3):291-301.
[17] Pi YL, Bradford MA, Tin-Loi F, Gilbert RI. Geometric and material nonlinear analysis of elastically restrained arches. Eng Struct 2007; 29(3):283-95.
[18] Pi YL, Trahair NS. Nonlinear buckling and postbuckling of elastic arches. Eng Struct 1998; 20(7):571-9.
[19] Pi YL, Trahair NS. In-plane buckling and design of steel arches. ASCE J Struct Eng 1999; 125(11):1291-8.
[20] Singer J, Arbocz J, Weller T. Buckling experiments: experimental methods in buckling of thin-walled structures. J Wiley. New York, USA. 1998.
[21] Spoorenberg RC, Snijder HH, Hoenderkamp JCD. A theoretical method for calculating the collapse load of steel circular arches. Eng Struct 2012; 38:89-103.
[22] Timoshenko S. Strength of materials part I: elementary theory and problems. 3rd ed. D Van Nostrand Co Inc. USA. 1930.
[23] Timoshenko SP, Gere JM. Theory of elastic stability. 2nd ed. McGraw-Hill. New York, USA. 1961.
[24] Williams A. Structural analysis: in theory and practice. Elsevier Butterworth–Heinemann Publications. USA. 2009.
[25] Wolde-Tinsaie AM, Foadian H. Asymmetrical buckling of prestressed tapered arches. ASCE J Eng Mech 1989; 115(9):2020-34.
[26] Yau JD, Yang YB. Geometrically nonlinear analysis of planar circular arches based on rigid element concept – a structural approach. Eng Struct 2008; 30(4):955-64.
[27] Ziemian RD. Guide to stability design criteria for metal structures. 6th ed. John Wiley & Sons Inc. New Jersey, USA. 2010.

7/22/2012